IEEE Photonics Journal
An IEEE Photonics Society Publication

A Multiband Transparent Transponder Based on Reconfigurable Optical Frequency Combs for Cross Connection of Intersatellite and Satellite Ground

Volume 10, Number 5, September 2018

Bin Wu
Hongxi Yin
Anliang Liu
Xiuyang Ji
Qingchun Zhao

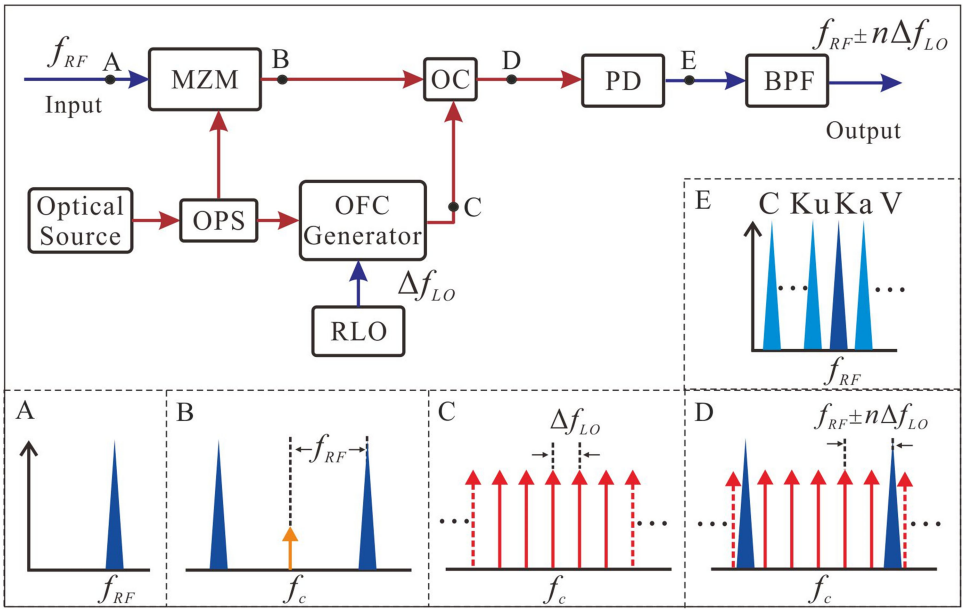

DOI: 10.1109/JPHOT.2018.2871041
1943-0655 © 2018 IEEE

A Multiband Transparent Transponder Based on Reconfigurable Optical Frequency Combs for Cross Connection of Intersatellite and Satellite Ground

Bin Wu,[1] **Hongxi Yin**,[1] **Anliang Liu**,[1] **Xiuyang Ji**,[1] **and Qingchun Zhao**[2]

[1]School of Information and Communication Engineering, Dalian University of Technology, Dalian 116023, China
[2]School of Computer and Communication Engineering, Northeastern University at Qinhuangdao, Qinhuangdao 066004, China

DOI:10.1109/JPHOT.2018.2871041

Manuscript received April 22, 2018; revised August 6, 2018; accepted September 14, 2018. Date of publication September 24, 2018; date of current version October 8, 2018. This work was supported in part by the National Natural Science Foundation of China under Grant 61871418 and Advanced Research Fund of General Armament Department under Grant 113030204-2. Corresponding author: Hongxi Yin (e-mail: hxyin@dlut.edu.cn).

Abstract: In this paper, a parallel multiband frequency-conversion scheme for satellite applications based on a single optical frequency comb is proposed, and a reconfigurable satellite transponder is designed for future multiband broadband satellites. In addition, we establish a test system of onboard multiband frequency-conversion on the strength of microwave photonics and, a proof-of-concept experiment is demonstrated in which a Ka-band signal is converted to other satellite frequency bands. The experimental results reveal our system feasibility, and the bit error rate of recovered baseband data is less than 10^{-9}. Moreover, the optical frequency combs can be reconfigured by adjusting the parameters of the local oscillator and optical modulator.

Index Terms: Microwave photonics, optical frequency comb, multi-band frequency conversion, reconfigurable satellite transponder.

1. Introduction

With the increasing demands of high-speed data communication in space, satellite navigation and positioning and high-resolution image acquisition from civil and military businesses, the satellite communication is driven to operate at higher frequency and larger bandwidth. Radio frequency (RF) transponders in communication satellites are now converting signals from C, Ku bands to Ka and even V bands [1], [2]. Simultaneously, to mitigate the frequency spectrum congestion and orbital resource depletion issues, the satellite coverage mode is transforming from single-spot to multi-spot coverage and multiple antennas are employed to transmit signals of different frequencies to implement communication of different services [3].

Under the increasing demand on multi-spot beam processing and forwarding in Ka band, satellite transponders are required to support the multi-channel switching, frequency conversion of different signals and the processing and regeneration of signals onboard. With the boosting of satellite

communication frequencies, the augmenting number of beams and the strengthening requirement for signal processing onboard, traditional transponders based on the frequency conversion in the electric domain encounter numerous issues, such as large payload size, heavy weight, high power consumption, low bandwidth and severe electro-magnetic interference (EMI), which has become a restricting bottleneck for broadband satellite communications [4], [5]. However, microwave photonic technique can effectively decrease the size, weight and power consumption of a satellite transponder and implement large bandwidth and ultra-high speed signal processing, and have turned into a trend of next generation system of high-frequency, multi-beam and large-capacity satellite communication [4], [6].

With respect to the satellite frequency conversion, the SAT'N LIGHT project of the European Space Agency (ESA) proposed the frequency down conversion of microwave signals with multiple optical local oscillators (LOs) based on the wavelength division multiplexing (WDM). However, the ability of multi-band communication is restricted by the frequency of the multiple optical LOs and the flexibility and reconfigurability are relatively poor [7]. A dual optical frequency comb (OFC) scheme using two OFCs with different frequency spacing to generate different frequency-bands by beating each pair of sidebands was proposed in [8]. Nonetheless, the conversion result is limited by fixed WDM channels and it is complicated to simultaneously control the system with two OFCs. In Ref. [9], a frequency conversion approach on the basis of a dual-polarization QPSK modulator was proposed and nevertheless, this work was simulation based only and not verified by experimental validation.

Therefore, based on the flexible bandwidth switching for a space information network in our previous work [10], we propose a novel multi-band frequency conversion scheme on basis of a single OFC for satellite applications in this paper. Furthermore, the mechanism of frequency conversion is analyzed and the structure of satellite transponder is designed. The system that can achieve the frequency conversion from a Ka-band signal to different bands simultaneously is designed and implemented experimentally. The experimental results indicate the frequency conversion ability of our satellite transponder and the feasibility to support multi-channel switching, frequency conversion of different signals and signal processing and regeneration of satellite payloads.

2. Structure and Function of Multi-Band Satellite Transponder

To meet the demand for multi-channel and multi-band satellite communication, the transparent satellite transponder unit with a function of multi-band frequency conversion is proposed and its schematic diagram is shown in Fig. 1. The relay transponder consists of an analog transparent transponder unit, a digital processor-based add/drop unit and an OFC generation unit. The analog transparent transponder unit receives signals of different frequency bands (S/C/Ku/Ka) from any LEO satellite or any ground station, and then, these signals are upconverted or downconverted to target frequencies in an optical domain. After the switching and analog processing, these output signals are transmitted transparently and their frequency bands match with those of destination nodes, such as a target satellite or a ground station. Hence, the transponder builds up a bridge among the satellites or ground stations of different bands.

Meanwhile, the node has the function of data regeneration and on-board processing. The switching unit can implement not only the cross connection of the microwave or radio frequency signals, but also the add/drop multiplexing. The transponders can downconvert a signal to an intermediate frequency (IF) and process the digital signal after sampling. Similarly, data generated locally can be upconverted to signals of different bands and then sent to the switching unit for processing.

The realization of the frequency conversion function onboard mentioned above is based on microwave photonics technique. The frequency conversion in the optical domain doesn't require a multi-level frequency conversion owing to the high carrier frequency, and simultaneously, can effectively avoid harmonic interference. Furthermore, the OFCs are employed for the all-optical frequency conversion of a received microwave signal [11]–[14] such that the multi-band, multi-channel parallel conversion can be implemented. The generation of OFCs is controlled by the reconfigurable local oscillator (RLO), whose frequency, amplitude and phase can be reconfigured

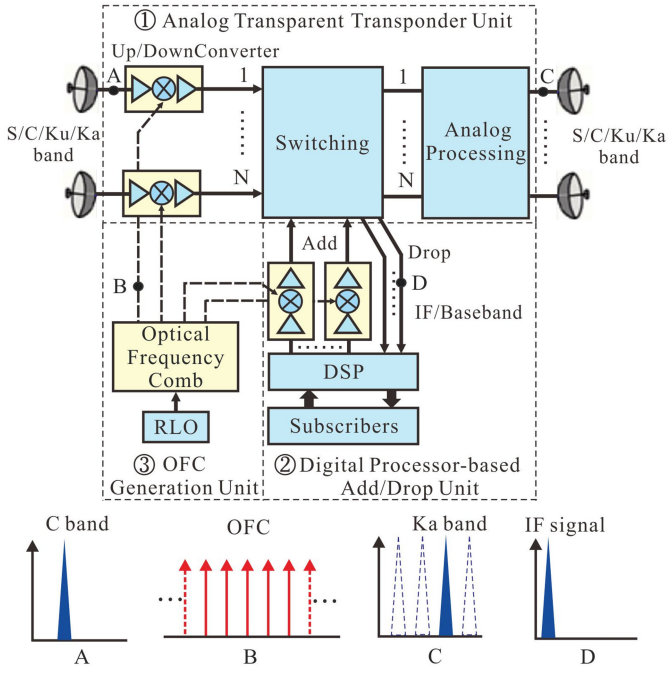

Fig. 1. Schematic diagram of multi-band satellite transponder unit. OFC: optical frequency comb, RLO: reconfigurable local oscillator, DSP: digital signal processing.

to control the central frequency, spacing and number of comb lines to meet the requirement of multi-band frequency conversion.

3. Multi-Band Frequency Conversions of Single-OFC

Compared to the traditional multi-level microwave frequency mixing, the multi-band frequency conversion node based on microwave photonics can support higher frequency-bands and provide stronger processing ability. Given that the frequency spacing of OFCs restrains the frequency range of output IF signals to a certain extent in [8], different order comb lines of the single OFC can beat with different frequency signals in a possibly wide range. Therefore, we propose a new multi-band frequency conversion scheme on the basis of single OFC, whose schematic is shown in Fig. 2.

Assume that the central frequency of an input RF signal from a certain channel is f_{RF}, shown in point A of Fig. 2. First, the local laser source of a satellite emits a beam of light with a central frequency f_c, which is divided into two ways by an optical power splitter (OPS). One light is employed as an optical carrier of the input RF signal with the frequency f_{RF}, to convert the received signal to an optical domain through a Mach-Zehnder modulator (MZM). The second laser path is exploited to produce an OFC through a reconfigurable electric LO (RLO) with a frequency Δf_{LO}. After these two optical signals are combined by an optical coupler (OC) the multi-band parallel output signal is obtained by frequency beating through a photodetector. Finally, the converted output signal of a corresponding frequency band is filtered out by an electric bandpass-filter according to an operating frequency band of a target satellite.

In order to convert the input RF signal to an optical domain through the MZM, its bias voltage is set at the minimum transmission point of its modulation curve ($V_{bias} = V_\pi + 2mV_\pi$, where m is an integer). The output optical signal at point B (shown in Fig. 2.) is generated by the double-sideband

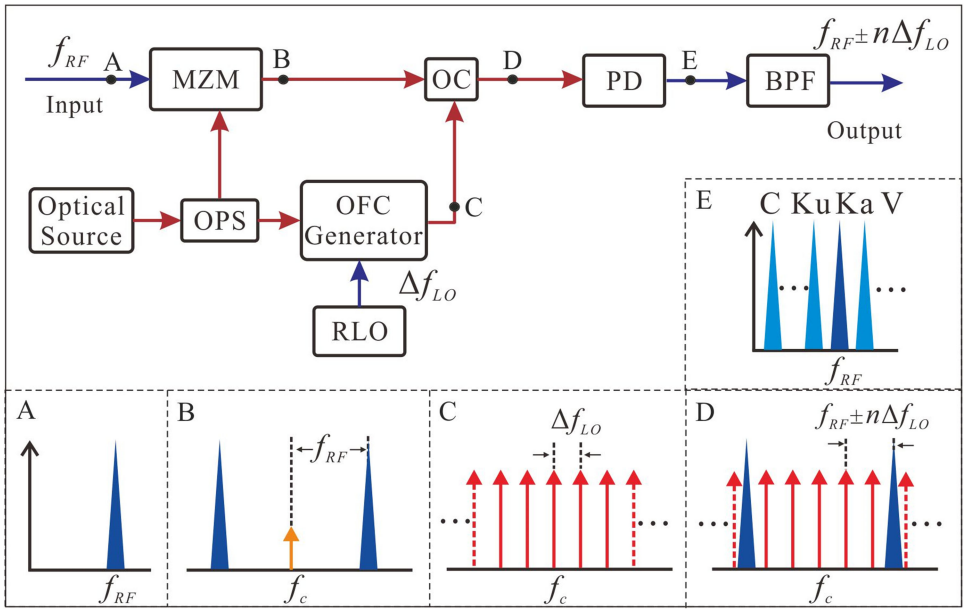

Fig. 2. Schematic diagram of multi-band frequency conversion based on microwave photonics. MZM: Mach-Zehnder modulator, OPS: optical power splitter, OC: optical coupler, PD: photodiode, BPF: band-pass filter.

suppressed-carrier (DSB-SC) modulation and its electrical field can be expressed as [15]

$$\begin{aligned} E_B(t) &= \frac{\sqrt{2}}{2} E_{in}(t) \sin\left(\frac{\pi V_{RF}\cos(\omega_{RF}t)}{2V_{\pi 1}}\right) \\ &= -\frac{\sqrt{2}}{2} E_{in}(t)\left[2\sum_{n=1}^{\infty}(-1)^n J_{2n-1}\left(\frac{\pi V_{RF}}{2V_{\pi 1}}\right)\cos((2n-1)\omega_{RF}t)\right] \\ n &= 1, 2\ldots \end{aligned} \tag{1}$$

where $E_{in}(t) = \sqrt{2P_{in}}e^{j\omega_c t}$ is the electrical field of the optical carrier, P_{in} is the output power of the laser, and ω_c is the angular frequency of the optical carrier. In (1), V_{RF} and ω_{RF} are the peak-to-peak voltage and angular frequency of the input RF signal for the MZM_1, respectively. $V_{\pi 1}$ is the MZM_1 switching voltage and $J_{2n-1}(\cdot)$ is the Bessel function of the first kind of order 2n − 1. When its higher-order sidebands are neglected and only the first harmonic component in (1) is retained, the output signal of the MZM_1 can be expressed as

$$E_B(t) = \sqrt{P_{in}}J_1\left(\frac{\pi V_{RF}}{2V_{\pi 1}}\right)\left[e^{j(\omega_c+\omega_{RF})t} + e^{j(\omega_c-\omega_{RF})t}\right] \tag{2}$$

Therefore, the upper and lower sideband frequencies of the MZM_1 output signal are $\omega_c + \omega_{RF}$ and $\omega_c - \omega_{RF}$, respectively.

Meanwhile, the light of the other path is sent to the OFC generation unit. In our scheme, the OFC is generated based on the single-stage dual-drive MZM (DD-MZM) modulator [16], and the comb spacing can be controlled by the RLO. Supposing that the angular frequency of the RLO is $\Delta\omega_{LO}$, the signal in point C of Fig. 2 can be signified as

$$E_C = \frac{1}{2}\sqrt{P_{in}}e^{j\omega_c t}\sum_{k=-\infty}^{\infty}\left[J_k\left(\frac{\pi V_{LO1}}{2V_{\pi 2}}\right)e^{j\left(k\Delta\omega_{LO}t+\frac{\pi V_{bias1}}{V_{\pi 2}}\right)} + J_k\left(\frac{\pi V_{LO2}}{2V_{\pi 2}}\right)e^{j\left(k\Delta\omega_{LO}t+\frac{\pi V_{bias2}}{V_{\pi 2}}\right)}\right] \tag{3}$$

where $V_{LO1,2}$ and $V_{bias1,2}$ are the peak-to-peak and DC bias voltages applied to two arms of the DD-MZM$_2$, respectively and $V_{\pi 2}$ is the DD-MZM$_2$ switching voltage. Assuming that $\theta_1 = \frac{\pi V_{bias1}}{V_{\pi 2}}$, $\theta_2 = \frac{\pi V_{bias2}}{V_{\pi 2}}$, $\beta_1 = \frac{\pi V_{LO1}}{2V_{\pi 2}}$ and $\beta_2 = \frac{\pi V_{LO2}}{2V_{\pi 2}}$, the power conversion from the input signal to the k-order harmonic mode can be asymptotically approximated as [17]

$$\eta = \frac{P_k}{P_{in}} = \frac{1}{2\pi\overline{\beta}}\left\{1 + \cos(\Delta\theta)\cos(2\Delta\beta) + [\cos(2\Delta\theta) + \cos(2\Delta\beta)]\cos\left(2\overline{\beta} - \frac{2k+1}{2}\right)\right\} \quad (4)$$

where $\Delta\theta = (\theta_1 - \theta_2)/2$, $\Delta\beta = (\beta_1 - \beta_2)/2$, and $\overline{\beta} = (\beta_1 + \beta_2)/2$ are the DC bias difference between the arms, the peak-to-peak phase difference induced in each arm of the DD-MZM$_2$ and the mean value of amplitude, respectively. When $\Delta\beta + \Delta\theta = n\pi \pm \frac{\pi}{2}$ is satisfied by adjusting the amplitude and DC bias voltage of the DD-MZM$_2$ input signal, the flat OFCs can be obtained from the output of the DD-MZM$_2$.

Presuming that the number of output OFC lines is $2N + 1$, the OFC signals are coupled with the upper DSB-SC signals, and then the electrical field in point D of Fig. 2 can be denoted as

$$E_D \propto \sqrt{P_{in}} J_1\left(\frac{\pi V_{RF}}{2V_{\pi 1}}\right)\left[e^{j(\omega_c+\omega_{RF})t} + e^{j(\omega_c-\omega_{RF})t}\right] + \sum_{n=-N}^{N}\sqrt{P_{in}}e^{j(\omega_c+n\Delta\omega_{LO})t} \quad (5)$$

A current produced by the total optical field in the photodetector satisfies the square law, given by

$$i(t) \propto R|E_D(t)|^2 \quad (6)$$

where R is the responsivity of the photodetector. By analyzing photocurrent $i(t)$ we can find that the current has three kinds of frequency components including $2\omega_{RF}$, $n\Delta\omega_{LO}$ and $\omega_{RF} \pm n\Delta\omega_{LO}$, where n is a positive integer.

Eventually, by setting a center frequency of the bandpass filter, the RF signal with the frequency of $f_{RF} \pm n\Delta f_{LO}$ is filtered output to complete the multi-band frequency conversion so that the matching with satellites operating at different bands is accomplished. By changing the frequency Δf_{LO} of the reconfigurable LO, it is possible to flexibly implement the switching among channels of the microwave satellite and to support the frequency conversion of C/Ku/Ka bands. In addition, from (5) and (6), we can deduce that the power of output signal is mostly determined by the output power of laser, modulation depth of the MZM and responsivity of the photodetector. Therefore, the conversion gain and signal to noise ratio (SNR) can be improved by increasing the input optical power of the photodetector.

4. Experimental Results for the Multi-Band Frequency Conversion System

According to our multi-band frequency conversion scheme on-board, an experimental system is established to test the frequency conversion ability of the satellite transponder and to verify the feasibility of the microwave photonic technique applied to an onboard processing. The structural diagram and photograph of the multi-band frequency conversion experiment are shown in Fig. 3(a) and (b).

Primarily, the Ka-band signal with the central frequency of 28 GHz is generated based on circuits developed by us, and then the signal is converted to the optical domain. The 500-Mbps baseband data with the pattern of $2^{31} - 1$ pseudo-random binary sequence (PRBS) is produced by the bit error rate tester (BERT) (Anritsu MP1800A). The baseband data are mixed with the 2 GHz and 26 GHz LO signals. After two upconversions, the upper sideband signal is filtered output by an amplifier and a bandpass filter. The Ka-band signal with the central frequency f_{RF} of 28 GHz is translated to the optical domain by the DSB-SC modulation. The electro-optical bandwidth of the modulator is 40 GHz (iXBlue MX-LN-40) and the DC bias voltage is set to V_π. The output signal with a frequency 28 GHz because of the frequency difference between the first order upper/lower sideband and the optical carrier, is obtained (point B in Fig. 3), and the output spectrum of the MZM$_1$ measured by an optical spectrum analyzer (Anritsu MS9740A) is shown in Fig. 4(a).

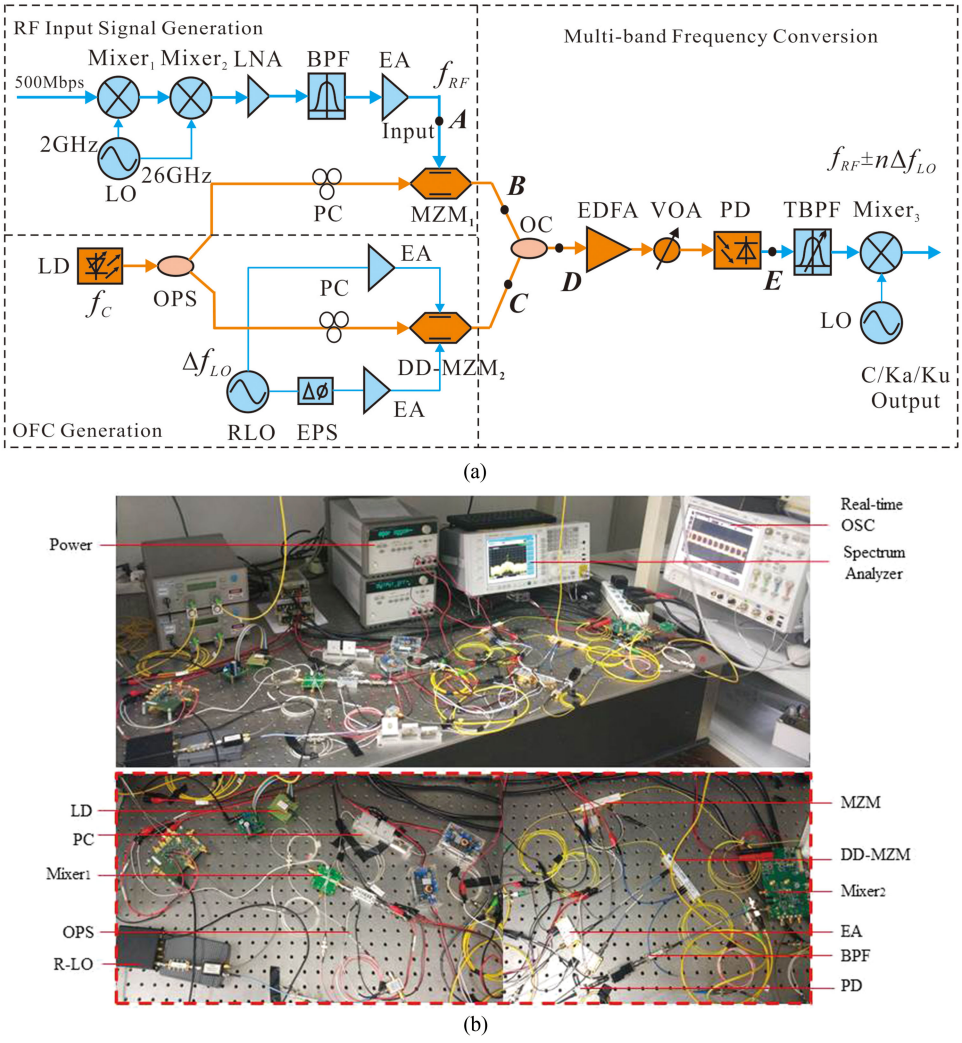

Fig. 3. Structural diagram and photograph of the multi-band frequency conversion experiment. (a) Structural diagram of the experimental system. (b) Identification experiment. LD: laser diode, PC: polarization controller, OPS: optical power splitter, RLO: reconfigurable local oscillator, MZM: Mach-Zehnder modulator, DD-MZM: dual-drive Mach-Zehnder modulator, OC: optical coupler, EA: electric amplifier, BPF: bandpass filter, PD: photodiode, LNA: low noise amplifier, VOA: variable optical attenuator, EDFA: Erbium-doped fiber amplifier, TBPF: tunable bandpass filter, OSC: oscilloscope.

Subsequently, the OFC generation unit outputs the photonic LO signal for the rear mixing. The OFC is generated by entering LO signals with different amplitudes to two arms of the DD-MZM$_2$. By configuring RLO's parameters of the reconfigurable LO source (DS SG6000L), the signals with frequencies of $\Delta f_{LO} = 13$ GHz and $2\,\Delta f_{LO} = 26$ GHz from the doubled-frequency ($\times 2$) and fourfold-frequency ($\times 4$) output ports, respectively. Through controlling the output port attenuation of the RLO, and the phase difference and DC bias voltages of two arms of the DD-MZM$_2$, the OFCs with different comb lines (n = 3, 4, 5) can be acquired. When its input signal voltages of the two arms are set to 3.8 V and 1.5 V and the DC bias voltage is set to 0.95 V, the OFC spectrum of the DD-MZM$_2$ output port is shown in Fig. 4(b). The number of the OFC comb lines is 5 and the comb line spacing is 13 GHz. Besides, the flatness of the OFC is 1.29 dB and its central wavelength is consistent with the spectrum of Fig. 4(a). Moreover, by adjusting parameters of the electrical LO and the optical modulator and thus changing the drive amplitudes of the RF signals, the phase between RF signals

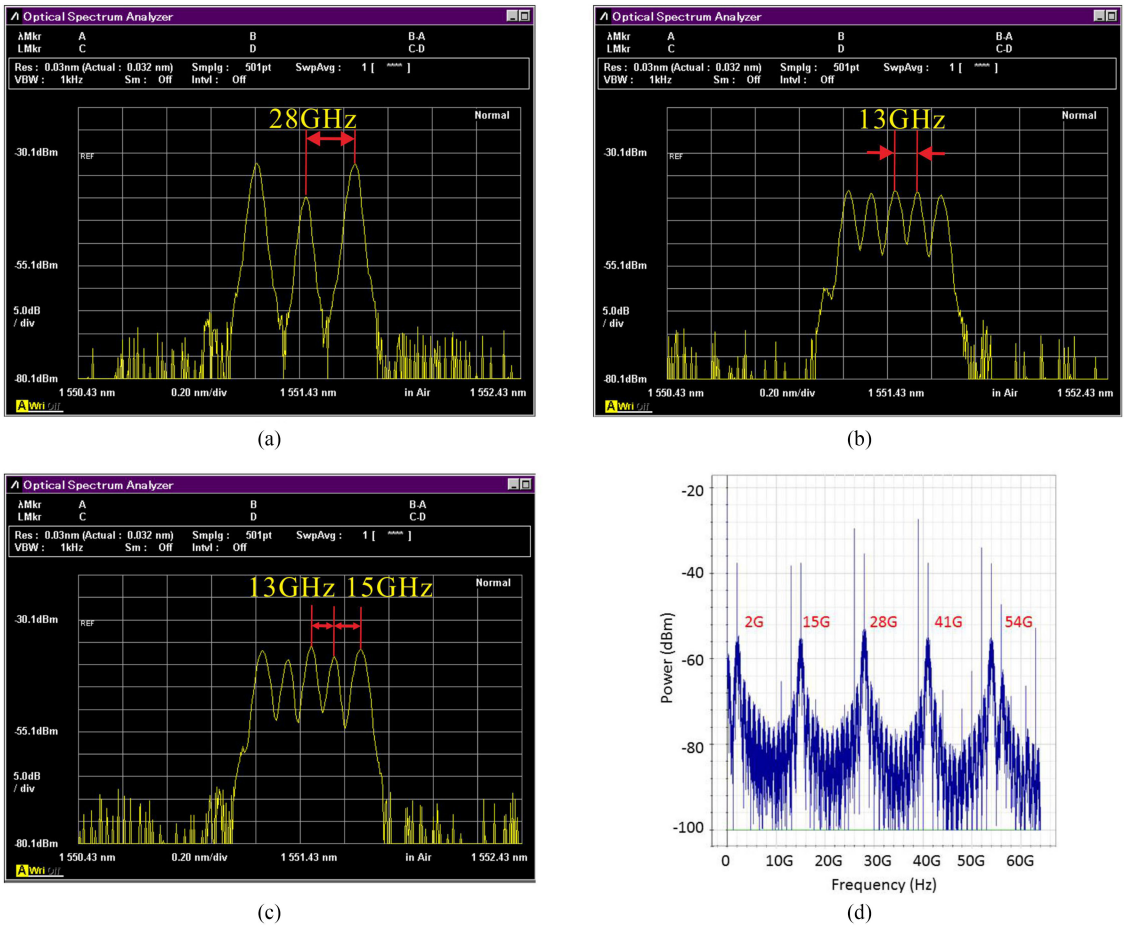

Fig. 4. Spectra of the output optical signal. (a) 28 GHz Ka-band signal. (b) OFC signal. (c) Optical signal after coupling. (d) Output spectrum after photodetection in the simulation.

TABLE 1
System Parameters: OFC Generation

Number of Comb Lines	Drive Amplitude of Arm-1 ($V_{\pi RF1}$)	Drive Amplitude of Arm-2 ($V_{\pi RF2}$)	DC Bias ($V_{\pi DC}$)	Flatness (dB)
3	0.71	0.23	0.69	0.97
4	0.98	0.52	0.50	1.20
5	1.52	0.60	0.54	1.29

and the optical carrier phase, the frequency spacing and the comb-line number of the OFC can be reconfigured and the wavelength offset can be changed by adjusting the wavelength of optical source. Adjusting the appropriate comb spacing and wavelength offset is one of the key steps in the frequency conversion. The parameters should be set to match with the desired satellite channels and bands to adapt the different communication tasks on satellites. The measurement results of the OFC generation under various system parameters are summarized in Table 1.

Finally, the multi-band frequency conversion unit converts the signal to a target frequency. The 28 GHz Ka-band signal modulated to the optical domain and the OFC signal with a frequency

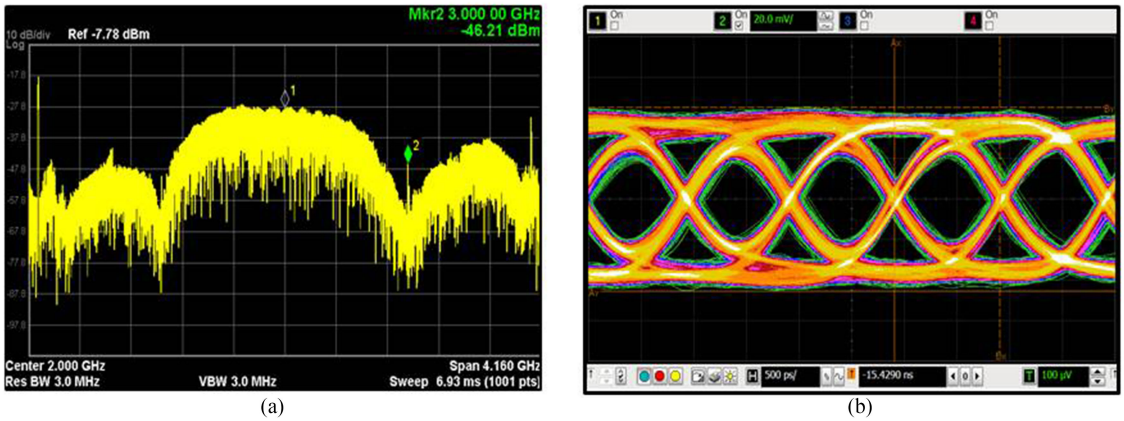

(a) (b)

Fig. 5. Spectrum and eye diagram of electrical signal after frequency conversion. (a) 2 GHz IF signal. (b) Eye diagram of the recovered baseband data.

spacing of 13 GHz are coupled into one path by the optical coupler (point D of Fig. 3) and its output optical spectrum is shown in Fig. 4(c). The frequency differences among the five peaks are 15 GHz, 13 GHz, 13GHz and 15 GHz, which are consistent with our theoretical analysis. After processed by the EDFA and the variable optical attenuator (VOA), the optical signal is sent to the 50 GHz bandwidth photodetector (Finisar XPDV2120) for a beat frequency. The electric current produced by the photodetector satisfies the square law and the 28 GHz signal (lower/upper sideband) beats the frequency of each comb lines with a frequency spacing of 13 GHz. Therefore, the frequencies of the output electrical signal (point E of Fig. 3) include many components ($28 \pm n \times 13$) such as 2 GHz, 15 GHz, 28 GHz and etc. Other frequency components with frequencies of 41 GHz and 54 GHz are unable to be measured owing to a limited measurement range of our signal analyzer. The spectrum in our theoretical simulation is shown in Fig. 4(d).

To simulate data received from target satellites or ground stations and verify the signal quality after the frequency conversion, the 2 GHz frequency component of the electrical signal is filtered output through a bandpass filter. The spectrum measured by a spectrum analyzer (Keysight N9020A) is shown in Fig. 5(a). The eye diagram of data recovered from the IF signal is shown in Fig. 5(b). When the data rate is 500 Mbps with test pattern lengths of $2^{31} - 1$, the bit-error rate (BER) is less than 10^{-9} measured by the BERT.

5. Conclusion

In this paper, we propose a structure of transparent transponder for inter-satellite relay and satellite-ground transmission, and a multi-band frequency conversion scheme for multi-beam satellite communications on account of a microwave photonics. Then, the mechanism of multi-band frequency conversion on the strength of single OFC is detailed and the generation and control of the OFC are discussed. Finally, we develop the circuits and establish an experimental test system to verify the abilities of multi-band frequency conversion and OFC reconfiguration. The experimental results indicate that the system can realize frequency conversion in the optical domain through the photoelectric mixer. It can simultaneously convert the Ka-band signal to other operational bands of satellites and the bit-error rate of the baseband data is less than 10^{-9}. Additionally, the OFC served as the optical LO signal for mixing is reconfigurable to satisfy the requirements of different satellite applications. Our frequency conversion structure is applicable to the convergence of multi-band and different frequency signals onboard in the future satellite networks and it has many benefits such as high efficiency and reliability, anti-interference and flexible applications.

References

[1] M. T. A. Panagopoulos, P. Arapoglou, and P. Cottis, "Satellite communications at Ku, Ka, and V bands: Propagation impairments and mitigation techniques," *IEEE Commun. Surveys Tuts.*, vol. 6, no. 3, pp. 2–4, Third Quarter 2004.

[2] G. Ziaragkas *et al.*, "SANSA hybrid terrestrial-satellite backhaul network: Scenarios, use cases, KPIs, architecture, network and physical layer techniques," *Int. J. Satell. Commun. Netw.*, vol. 35, no. 5, pp. 379–404, Sep. 2007.

[3] E. Lutz, "Towards the terabit/s satellite—Interference issues in the user link," *Int. J. Satell. Commun. Netw.*, vol. 34, no. 4, pp. 461–482, Jul. 2016.

[4] S. Pan *et al.*, "Satellite payloads pay off," *IEEE Microw. Mag.*, vol. 16, no. 8, pp. 61–73, Sep. 2015.

[5] B. Roy *et al.*, "Optical feeder links for high throughput satellites," in *Proc. IEEE Int. Conf. Space Opt. Sys. Appl.*, Oct. 2015, pp. 1–6.

[6] J. Yao, "Microwave photonics," *J. Lightw. Technol.*, vol. 27, no. 1-4, pp. 314–335, Jan. 2009.

[7] M. Sotom, B. Benazet, A. Le Kernec, and M. Maignan, "Microwave photonic technologies for flexible satellite telecom payloads," in *Proc. 35th Eur. Conf. Opt. Commun.*, Sep. 2009, pp. 1–4.

[8] X. Yang *et al.*, "Optical frequency comb based multi-band microwave frequency conversion for satellite applications," *Opt. Exp.*, vol. 22, no. 1, pp. 869–877, Jan. 2014.

[9] T. Lin, S. Zhao, Q. Zheng, Z. Zhu, X. Li, and K. Qu, "Photonic microwave multi-band frequency conversion based on a DP-QPSK modulator for satellite communication," *Opt. Rev.*, vol. 24, no. 3, pp. 310–317, Jun. 2017.

[10] B. Wu, H. Yin, A. Liu, C. Liu, and F. Xing, "Investigation and system implementation of flexible bandwidth switching for a software-defined space information network," *IEEE Photon. J.*, vol. 9, no. 3, Jun. 2017, Art. no. 5502114.

[11] Y. Dou, H. Zhang, and M. Yao, "Improvement of flatness of optical frequency comb based on nonlinear effect of intensity modulator," *Opt. Lett.*, vol. 36, no. 14, pp. 2749–2751, Jul. 2011.

[12] Q. Wang, L. Huo, L. Y. Xing, and B. Zhou, "Ultra-flat optical frequency comb generator using a single-driven dual-parallel Mach–Zehnder modulator," *Opt. Lett.*, vol. 39, no. 10, pp. 3050–3063, May 2014.

[13] C. He, S. Pan, R. Guo, Y. Zhao, and M. Pan, "Ultraflat optical frequency comb generated based on cascaded polarization modulators," *Opt. Lett.* vol. 37, no. 18, pp. 3834–3836, Sep. 2012.

[14] P. Bardella, L. Columbo, and M. Gioannini, "Self-generation of optical frequency comb in single section quantum dot Fabry-Perot lasers: A theoretical study," *Opt. Exp.*, vol. 25, no. 21, pp. 26234–26252, Oct. 2017.

[15] V. Thomas, M. El-Hajjar, and L. Hanzo, "Millimeter-wave radio over fiber optical upconversion techniques relying on link nonlinearity," *IEEE Commun. Surveys Tuts.*, vol. 18, no. 1, pp. 29–53, Firstquarter 2016.

[16] N. Yokota, T. Miki, K. Abe, and H. Yasaka, "Nonlinearity of semiconductor Mach-Zehnder modulator for flat optical frequency comb," *IEEE Photon. Technol. Lett.*, vol. 27, no. 21, pp. 2219–2221, Nov. 2015.

[17] A. Hraghi, M. Chaibi, M. Menif, and D. Erasme, "Demonstration of 16QAM-OFDM UDWDM transmission using a tunable optical flat comb source," *J. Lightw. Technol.*, vol. 35, no. 2, pp. 238–245, Jan. 2017.